Materials Advances

ROYAL SOCIETY OF CHEMISTRY

PAPER

View Article Online
View Journal | View Issue

Cite this: *Mater. Adv.*, 2022, 3, 6485

Ionic liquid based dopant-free band edge shift in $BiVO_4$ particles for photocatalysis under simulated sunlight irradiation†

Niqab Khan,*[a] Rogério Nunes Wolff,[a] Hameed Ullah,[a] Gustavo J. Chacón,[b] Washington Santa Rosa,[c] Jairton Dupont,[b] Renato Vitalino Gonçalves[c] and Sherdil Khan*[a]

Foreign elemental doping is a widely utilized strategy to modify the electronic structure of semiconductors. Herein, we present a dopant-free novel synthesis approach to control the electronic structure of a semiconductor. Utilizing butyl methyl imidazolium ([BMIM]Cl) and methoxyethyl methyl imidazolium ([M(MOE)Im][Cl]) chloride ILs, we prepared four different Bi and V based ILs: 3-butyl-1-methyl-1*H*-imidazol-3-ium vanadate [BMIm][VO_3], 3-(2-methoxyethyl)-1-methyl-1*H*-imidazol-3-ium vanadate [M(MOE)Im][VO_3], 3-butyl-1-methyl-1*H*-imidazol-3-ium tetrachlorobismate [BMIm][$BiCl_4$] and 3-(2-methoxyethyl)-1-methyl-1*H*-imidazol-3-ium tetrachlorobismate [M(MOE)Im][$BiCl_4$]. Owing to the bimetallic oxide nature of $BiVO_4$, these gels were mixed either with each other or with Bi/V commercial salts and simply heat-treated to obtain monoclinic $BiVO_4$. Depending on the IL, the bandgap energy of pure $BiVO_4$ will be redshifted (2.44 to 2.25 eV). The IL based synthesis induced oxygen vacancies and uplifted the $BiVO_4$ valence band edge as observed in the X-ray photoelectron spectroscopy (XPS). These effects were profound for IL anchored Bi; however, the side effects of this synthesis were chemisorption of a higher oxygen content and low reactivity of Bi with V to form an additional V_2O_5 phase. ILs acted as templates to form smooth spherical particles with improved crystallinity. [M(MOE)Im] based synthesis resulted in lower-order crystallinity and a large V–O bonding length of $BiVO_4$ compared to [BMIm] which may be ascribed to its lower-order cationic–anionic electrostatic attraction associated with the presence of oxygen in the ether-group for [M(MOE)Im]. [BMIm] cation-based synthesis suppressed photogenerated charge-recombination and resulted in a five-fold O_2 evolution of ~30 μmol for 3 h (AM 1.5G illumination) compared to pure $BiVO_4$ which was better compared to the sample prepared by the conventional hydrothermal process. It also improved the photocurrent, and the MS plots have shown that the conduction band was not much affected; however, the defect density was larger for IL based synthesis.

Received 4th March 2022,
Accepted 29th May 2022

DOI: 10.1039/d2ma00259k

rsc.li/materials-advances

1. Introduction

The environmental pollution and rising CO_2 level in the atmosphere due to the consumption of fossil fuels are significant challenges for mankind.[1–4] The total energy consumption by all humans over a year is less than the solar energy that the Earth receives in one hour.[3–6] However, the main challenge lies in developing devices that convert solar energy to other forms of energy. A photocatalytic approach that utilizes solid–liquid interfaces for energy harvesting under sunlight is promising because of its simplicity and environment-friendly use of solar energy.[7,8]

Many semiconducting photocatalytic materials such as metal oxides, ternary oxides, nitrides, halides, and sulfides have been developed for energy and environmental applications due to their promising photocatalytic activities and non-toxicity.[9–14] Among these photocatalysts, bismuth vanadate ($BiVO_4$) is of crucial importance due to its outstanding features, such as a low bandgap (~2.4 eV), a maximum photocurrent density of 7.5 mA cm^{-2}, ~9% of solar to hydrogen conversion efficiency, excellent dispersibility, non-toxicity, high resistance to corrosion and promising photocatalytic activity under visible

[a] *Laboratory of Nanomaterials for Renewable Energy and Artificial Photosynthesis (NanoREAP), Federal University of Rio Grande do Sul (UFRGS), Campus do Vale, Agronomia, Porto Alegre-RS, Brazil. E-mail: sherdil.khan@ufrgs.br, sherdiljadoon@gmail.com*

[b] *Laboratory of Molecular Catalysis (LAMOCA), Federal University of Rio Grande do Sul (UFRGS), Campus do Vale, Agronomia, Porto Alegre-RS, Brazil*

[c] *São Carlos Institute of Physics, University of São Paulo, PO Box 369, 13560-970 São Carlos, SP, Brazil*

† Electronic supplementary information (ESI) available: SEM and XRD analyses, BET and XPS spectra. See DOI: https://doi.org/10.1039/d2ma00259k

light illumination.[15–17] $BiVO_4$ crystalizes in three phases, namely, tetragonal zircon, tetragonal scheelite, and monoclinic scheelite, of which monoclinic scheelite presents excellent photoactivity.[18] Besides these interesting features, $BiVO_4$ also presents disadvantages such as a low electron mobility, slow water oxidation kinetics,[19] lower electron transport,[20] and high charge recombination.[21,22] The preceding literature deals with some strategies to circumvent these limits. The most common available strategies are doping, surface modification with water oxidation co-catalysts, heterojunction formation, and morphological fine tuning.[23–25] Doping $BiVO_4$ with other metals improved the charge kinetics, electron conductivity, and light absorption due to the modification of its electronic structure.[20,26] For example, Zhou *et al.* synthesized $BiVO_4$ using Mo dopants which optimized the charge carrier densities and electron mobility.[27] Abdi *et al.* introduced tungsten (W) as a dopant to $BiVO_4$, which helped to improve charge separation and transport.[28] Shi *et al.* formed a $BiVO_4$ heterojunction with WO_3 which improved the electron/hole transfer.[29] Furthermore, hydrothermal synthesis is widely utilized to synthesize $BiVO_4$; although it is simple and can also be used to dope $BiVO_4$ with other metals, it is challenging to achieve large-scale synthesis based on this process. Thus, it is important to develop alternative dopant free synthesis routes that are capable of fine-tuning the electronic structure of $BiVO_4$ and have the capacity for large-scale preparation.

Ionic liquids (ILs) are molten salts used to synthesize many inorganic nanomaterials because of their key characteristics: high thermal stability, excellent dissolving power, a wide electrochemical window, ionic conductivity, and negligible vapor pressure.[30–34] ILs act as solvents and provide a template framework to produce ordered nanostructures during synthesis; particularly, the cationic interaction with the framework species is the main reason for their solid templating effect.[35] In addition to these tremendous benefits, recent studies report on modification of the electronic structure of semiconductors due to their interaction with ILs. Theoretical studies by Weber *et al.* have shown that the band edges of a semiconductor such as TiO_2 can be fine-tuned by the IL interaction. They emphasized on the charge transfer nature between both; thus, the cation stimulates an energetic downward shift of band levels by accepting and the anions raised the energy levels by donating electrons from the surface, thus improving its photoactivity.[36,37] However, TiO_2 is a UV absorbing semiconductor. Therefore, attempts are warranted to modify the energy bands of other visible light absorbing semiconductors *via* IL assisted synthesis. Structural defects, particularly, oxygen vacancies, play an essential role in the photocatalytic performance of $BiVO_4$.[38,39a] Earlier in the literature, ILs such as [EMIM]I and [BMIM]Cl were added directly in the synthesis of $BiVO_4$ based heterostructures by impregnation.[39b,c] However, the effect of ILs on the band edges of $BiVO_4$ was not explored which is crucial to understand the electronic properties of $BiVO_4$. The conduction band (CB) and valence band (VB) of $BiVO_4$ are mainly composed of V 3d and Bi 6s states, respectively, and ILs exhibit a unique benefit that they can be anchored to Bi and/or V sides to produce respective precursor gels which can be used to prepare $BiVO_4$ to control its electronic structure.

In this work, instead of direct physical mixing of ILs in $BiVO_4$ synthesis, we firstly prepared four newly imidazolium-based bismuth and vanadium precursor ILs ([BMIm][VO_3], [M(MOE)Im][VO_3], [BMIm][$BiCl_4$] and [M(MOE)Im][$BiCl_4$]). These precursors were mixed in a novel fashion to prepare $BiVO_4$. The photocatalytic response of the prepared materials was tested for oxygen evolution in photolysis and PEC setups under simulated solar irradiation.

2. Experimental

2.1. Materials

All reagents were used without further purification and purchased from Sigma-Aldrich. All experiments were conducted under normal atmospheric conditions.

2.2. Synthesis of precursor ILs, bismuth and vanadium composites

1-Butyl-3-methylimidazolium chloride [BMIm][Cl] and 1-(2-methoxyethyl)-3-methylimidazolium chloride [M(MOE)Im][Cl] were prepared following previous reports.[33,40] [BMIm][VO_3] (**IL1**) and [M(MOE)Im][VO_3] (**IL2**) were prepared by anion exchange, *i.e.* separately, a solution of water containing 5 g of [BMIm][Cl] or [M(MOE)Im][Cl] was passed through an AmberSep (900 OH) column to obtain the corresponding hydroxide-anion based ILs. Afterward, 1.87 g of NH_4VO_3 was added to these IL aqueous solutions and stirred for 16 hours at room temperature. To obtain **IL1** and **IL2** (Fig. 1), the resulting yellow solutions were transferred to a rotary evaporator in order to extract the formed ammonium species and the residual water (3.82 g) from the solution.

For the synthesis of [BMIm][$BiCl_4$] (**IL3**) and [M(MOE)Im]-[$BiCl_4$] (**IL4**), firstly ($Bi(NO_3)_3{\cdot}5H_2O$) (2.91 g; 0.006 mol) was calcined at 500 °C for 5 h at a 5 °C min^{-1} heating rate to obtain Bi_2O_3 (1.45 g; 0.003 mol). Afterward, 1 mL of concentrated HCl was added to the flask and stirred for 20 h to obtain a pale-yellow solution which was then dried off using a rotary evaporator until the formation of a characteristic white solid of $BiCl_3{\cdot}2H_2O$. Finally, 500 mg of this solid was added separately to equimolar amounts of [BMIm][Cl] (248 mg; 1.42 mmol) and [M(MOE)Im][Cl]

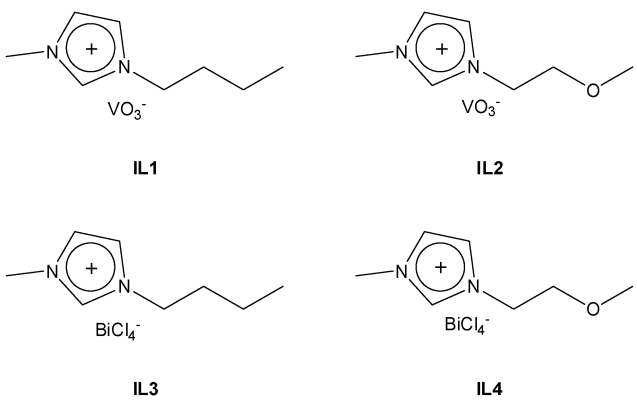

Fig. 1 Chemical structures of different ILs synthesized in this work.

(251.35 mg; 1.42 mmol) which resulted in the formation of **IL3** and **IL4**, respectively (Fig. 1).

2.2.1. Syntheses of $BiVO_4$

Route 1. **IL1** and **IL2** were used as vanadium precursors, and $Bi(NO_3)_3{\cdot}5H_2O$ was used as a bismuth precursor. 500 mg of the corresponding ILs were added to 0.98 g of Bi $(NO_3)_3{\cdot}5H_2O$ dissolved in 5 mL of dimethyl sulfoxide (DMSO). The resulting gel was stirred until the color of the solution was changed to red and then calcined at 500 °C for 5 h at a 5 °C min^{-1} heating rate to obtain a bright yellow $BiVO_4$ powder. For simplicity, we denote these samples as Bi:[V–Bm] and Bi:[V–Me], where Bm and Me represent [BMIm] and [M(MOE)Im], respectively.

Route 2. In this experiment, we mixed stoichiometric amounts of V and Bi anchored ILs as precursors. In a 25 mL round bottom flask, 300 mg (1.26 mmol) of **IL1** and 617 mg (1.26 mmol) of **IL3** were dissolved in 3 mL DMSO and stirred until the color of the solution changes to red. Afterward, the solution was calcined in a furnace at 500 °C for 5 h at a 5 °C min^{-1} heating rate to form a yellow powder. The same procedure was followed for **IL2** (300 mg; 1.26 mmol) and **IL4** (615 mg; 1.26 mmol). These samples are named [Bi–Bm]:[V–Bm] and [Bi–Me]:[V–Me] where Bm and Me represent [BMIm] and [M(MOE)Im], respectively. Schematically, the synthesis procedure is shown in Scheme 1.

For comparison, we prepared $BiVO_4$ without ILs. Equimolar amounts of $Bi(NO_3)_3{\cdot}5H_2O$ and NH_4VO_3 were mixed in the presence of deionized water and stirred for 30 min. The yellow precipitants were washed with deionized water and dried at 80 °C for 6 h. Finally, the obtained powder was calcined at 500 °C for 3 h at a 5 °C min^{-1} heating rate to obtain $BiVO_4$ and is named pure $BiVO_4$. For hydrothermal synthesis, $Bi(NO_3)_3{\cdot}5H_2O$ was dissolved in 10 mL of CH_3COOH and NH_4VO_3 in 50 mL of deionized water. After 30 min of separate stirring, the $Bi(NO_3)_3{\cdot}5H_2O$ solution was added to the NH_4VO_3 solution and stirred for an additional 1 h while keeping the pH ≈ 6 using NaOH. The entire solution was shifted to a 100 mL autoclave and placed inside an oven at 150 °C for 10 h at a 5 °C min heating rate. The obtained yellow powder was decanted by centrifugation, washed with ethanol, and dried at 80 °C for 6 h. This sample is named HT-$BiVO_4$.

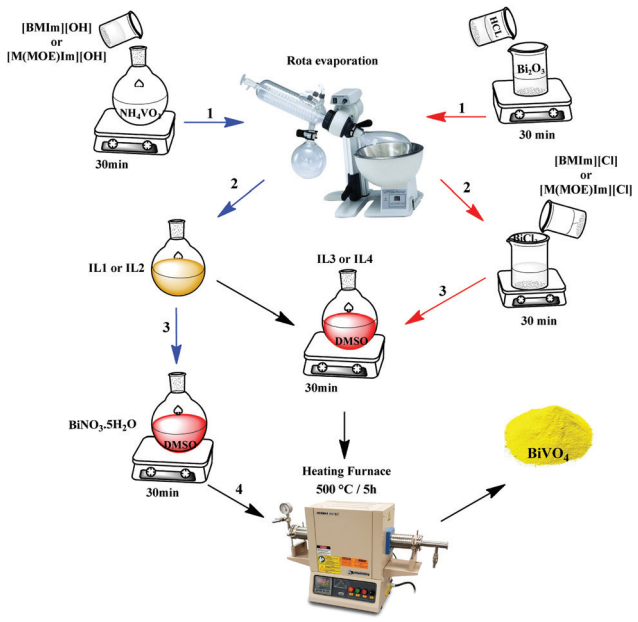

Scheme 1 Synthesis of IL-based $BiVO_4$: the Cl anion was exchanged for VO_3 and $BiCl_4$ in the ILs (steps 1–3). Once prepared, **IL1–IL4** were utilized as V and Bi precursors, respectively. These precursors were either mixed with each other or with Bi and V commercial salts to synthesize $BiVO_4$.

2.3. Characterization

The structure of the prepared powder samples was characterized using an X-ray diffractometer (X'Pert MPD) operating at 45 kV and 40 mA using Cu-Kα radiation. XRD was recorded in the 2 theta range of 10° to 60° with a step size of 0.05°. Ultraviolet-visible (UV-Vis) diffuse reflectance spectra were obtained to investigate the band gap of the photocatalyst using a Shimadzu UV-2600. The morphology was studied by field emission gun scanning electron microscopy (FEG-SEM) using a JEOL 7000F FEG-SEM operating at 10 kV. Raman spectra were obtained by using a Renishaw inVia Raman microscope equipped with a dual CCD camera and an Ar–Kr laser source of 514 nm wavelength. The specific surface area was measured according to the Brunner–Emmett–Teller (BET) method using a Micromeritics Tristar 3000 (hydrogen adsorption at 77 K). The average pore size was determined from the thermal desorption of N_2 using BJH analysis. The PL spectra were recorded using a Hitachi spectrofluorometer (model: F-4500). X-ray photoelectron spectroscopy (XPS) was used to analyze the electronic surface composition (Scienta Omicron ESCA+, Al Kα source) by using a low-energy electron flood gun for charge compensation. Scans were collected for a pass energy of 50 eV with energy steps of 0.5 eV for survey spectra and 0.05 eV for high resolution spectra. The binding energy of adventitious carbon (C–C at 284.8 eV) was used to calibrate the XPS spectra, and data analysis was performed using CasaXPS software, applying the line shape of GL(30) for peak fitting.

2.4. Photocatalytic oxygen evolution

Oxygen (O_2) evolution was carried out in an 86 mL air-tight quartz reactor directly connected to a gas chromatograph. 25 mg of the sample was dissolved in an aqueous solution of 0.05 M $Fe(NO_3)_3{\cdot}9H_2O$. Before photolysis, the samples were dispersed properly in the aqueous solution using the sonication method for 10 min. Argon gas was bubbled into a quartz reactor for 15 min to remove dissolved gases. The quartz reactor was connected to an airtight setup, the surface air was removed through a vacuum, and the space in the quartz reactor was filled with argon. Subsequently, the solution was kept under stirring and irradiated using a 300 W Xe lamp (PerkinElmer; Cermax PE300) with an AM 1.5G filter. Oxygen evolution was detected automatically at 1 h intervals in an Agilent gas chromatograph (model: 7890B) for 3 h using a Porapak-Q column 80/100 mesh equipped with a thermal conductivity detector (TCD) and connected in series with a FID.[41]

2.5. Photoelectrochemical (PEC) measurements

For PEC measurements, samples were prepared by spin coating on FTO glass substrates by adding 9 layers of $BiVO_4$. The choice of 9 layers was based on Fig. S8 (ESI†), where 9 layers of the thick film resulted in an improved PEC performance. Equimolar amounts (3 mmol) of Bi $(NO_3)_3{\cdot}5H_2O$ and NH_4VO_3 were mixed in the presence of 5 mL of dimethyl sulfoxide (DMSO) to form a slurry, and for each layer, a 100 μL drop of the prepared solution was added on FTO at an initial spinning rate of 500 rpm for 5 s and then at 3000 rpm for 10 s. The sample was set to dry at 150 °C for 25 min, and then the procedure was repeated 9 times; this sample is denoted as $BiVO_4$. To prepare the IL-based photoelectrode, a 100 μL drop of the IL [BMIm] $[VO_3]$ was added on the top layer of $BiVO_4$ by spin coating under the same conditions mentioned above (for simplicity, this sample is named BMIM-$BiVO_4$). These samples were heat-treated at 500 °C for 2 h at a heating rate of 5 °C min^{-1}. The electrodes were insulated using epoxy resin, and the ohmic contact was established using silver paste with a copper wire. The measurements were performed in an Autolab potentiostat. Linear sweep voltammetry (LSV) curves were recorded under AM 1.5G illumination (100 mW cm^{-2}) with a 300 W Xe lamp as the illumination source using an aqueous solution of 0.2 M Na_2SO_3 and 0.25 M phosphate buffer as the electrolyte. Mott–Schottky curves were recorded at a frequency of 1000 Hz in the same electrolyte. The electrolyte was purged with Ar for 30 min prior to the measurements.

3. Results and discussion

Fig. 2a displays the XRD patterns of the prepared samples. The XRD peaks are in good agreement with the standard Joint Committee on Powder Diffraction Standards (JCPDS) Card No. 14-0688 (space group: $I2/a$, a = 5.195, b = 11.701, c = 5.092, b = 90.38) corresponding to monoclinic-scheelite (m-s) $BiVO_4$.[42] For samples [Bi–Bm]:[V–Bm] and [Bi–Me]:[V–Me], some small peaks at $2\theta \sim 20°$, 26°, and 31° were also observed, which are the characteristic peaks of vanadium oxide (V_2O_5).[43] These results indicate that inserting the IL into Bi and V sides simultaneously hampers the complete formation of $BiVO_4$. Anchoring both metals with the IL increases the amount of IL in the synthesis matrix which may hinder their solid–solid diffusion for complete phase transformation to $BiVO_4$. In addition, we cannot ignore if the formation of V_2O_5 was solely due to the Bi interaction with the IL. Thus, we prepared [Bi–Bm]:V in which IL anchored Bi was used as the Bi precursor and NH_4VO_3 was used as the V precursor. It can be seen (Fig. S1a, ESI†) that, compared to [Bi–Bm]:[V–Bm] and [Bi–Me]:[V–Me] (Fig. 2a), this sample presents higher relative intensity peaks of V_2O_5. The internal anion interaction between Bi and Cl is less polar and more covalent which may be the reason for the lower reactivity between Bi and V.[44] Therefore, we may suggest that adding the IL on the Bi side decreases the interaction between Bi and V to form $BiVO_4$, and as a result the reaction is stabilized to obtain an additional unwanted phase of V_2O_5 under calcination conditions.[45,46] The Scherrer formula was used to estimate the crystal size:[47]

$$D = \frac{K\lambda}{\beta \cos\theta} \quad (1)$$

where D represents the crystal size in nanometers, K is the shape factor, λ is the X-ray wavelength (0.15418 nm), and β is the peak width at half maximum. The physical properties (crystallinity and crystallite size) were obtained from the XRD analyses (Table S1, ESI†). For the sample without ILs, the grain size was the smallest, and compared to other samples its baseline is not smooth, indicating lower order crystallinity (Fig. 2a and Table S1, ESI†). On the other hand, all IL based syntheses resulted in improved crystallinity and a larger grain size. Thus, the presence of ILs in the synthesis improves the crystal structure. In addition, the effect of the cation on the crystal size and crystallinity is noteworthy; compared to Bi:[V–Me], improved crystallinity was observed for Bi:[V–Bm] (Table S1, ESI†).

The Raman spectra of different $BiVO_4$ samples are compared in Fig. 2b. Typical vibrational bands (~324, 366, 640, 710, and 826 cm^{-1}) are observed for all $BiVO_4$ samples. Raman bands observed at 324 and 366 cm^{-1} for all samples correspond to the VO_4 tetrahedron characteristics, whereas the Raman band at 640 cm^{-1} corresponds to the asymmetric stretching of the

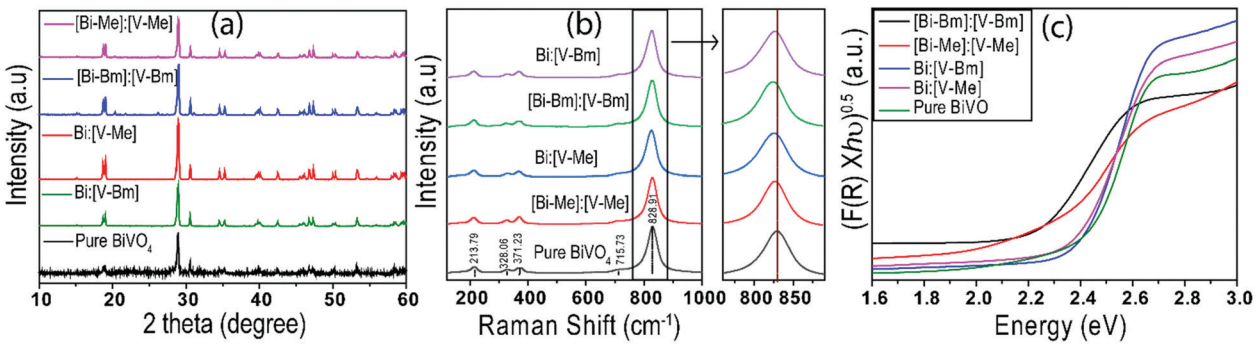

Fig. 2 (a) XRD patterns of $BiVO_4$ samples synthesized using [BMIm] and [M(MOE)Im] based ionic liquids in comparison to the sample without ILs (pure $BiVO_4$); (b) Raman spectra of $BiVO_4$ samples synthesized using the ionic liquid and pure $BiVO_4$ obtained at an excitation wavelength λ of 648 nm; the inset highlights the higher intensity peaks with their respective peak shifts relative to pure $BiVO_4$; (c) UV-vis absorption spectra of the samples synthesized using ionic liquids, showing a clear red-shift in the bandgaps compared to pure $BiVO_4$.

shorter V–O bond. Similarly, bands at 710 and 826 cm^{-1} provide information about V–O bond lengths.[48,49] Different shifts in the peaks have been observed for the samples synthesized using ionic liquids (Fig. 2b). In the literature, the shift in peaks is correlated to the V–O bond length, which can be obtained by using eqn (2):[49]

$$\nu\ (cm^{-1}) = 21\,349 \exp(-1.9176R\ (Å)) \quad (2)$$

where ν is the Raman frequency for the V–O bond and R is the bond length in angstrom. The bond lengths are compared in Table S2 (ESI†). V–O bond lengths for Bi:[V–Me] and Bi:[V–Bm] are 1.6971 Å and 1.6961 Å, respectively, and for Bi:[V–Me], the bond length is slightly longer than that of Bi:[V–Bm], and also for [Bi–Me]:[V–Me], it is increased when compared to [Bi–Bm]:[V–Bm] (Table S2, ESI†). These results indicate that [M(MOE)Im] based synthesis gave rise to an increase in the V–O bond length in contrast to [BMIm] for its individual anchoring with V or for both Bi and V when compared to their counterparts of [BMIm]. The UV-Vis spectra of the samples are compared in Fig. 2c. Compared to pure $BiVO_4$, the presence of ILs clearly red-shifted the bandgap energy (Table S2, ESI†). The largest bandgap shift was observed for [Bi–Bm]:[V–Bm], followed by [Bi–Me]:[V–Me], Bi:[V–Me] and Bi:[V–Bm], respectively. A similar red shift is observed when the IL is added only on the Bi side (Fig. S1b, ESI†). These results indicate that anchoring the IL on the Bi side greatly affects the optical properties of $BiVO_4$ compared to its individual addition to the V side. Thus, the light absorbance of $BiVO_4$ can be controlled *via* IL based synthesis. Generally, a shift in the bandgap is observed *via* doping with foreign elements, *e.g.* Wang *et al.* used europium as a dopant and observed a red shift from 2.43 eV to 2.26 eV,[50a] and Zhou *et al*. used Co as a dopant and observed a shift from 2.43 eV to 2.27 eV.[26] Our results clearly indicate that another simple way to modify the electronic structure of $BiVO_4$ is the IL based synthesis which is promising as it is dopant-free and it does not need a hydrothermal approach to produce doped or undoped $BiVO_4$.

IL based synthesis of $BiVO_4$ resulted in the formation of structures with smooth and regular spherical morphology compared to the sample without ILs (Fig. S2 (ESI†) and Fig. 3), showing that ILs act as structuring agents for an ordered and controlled nucleation of the $BiVO_4$ structure. ILs offer low interfacial tension and a high nucleation rate to enable the formation of ordered particles with improved crystallinity.[39c,50b] The particle size was measured for all samples while selecting more than a hundred particles randomly (Table S1, ESI†).[50c] Compared to ~1 μm sized Bi:[V–Me], a much smaller particle size of ~221 nm was obtained for Bi:[V–Bm], and we suggest that these size differences are due to higher intermolecular Bi–O interactions caused by the presence of a methoxy group in the lateral chain for [M(MOE)Im], which probably increases the interstitial space, and therefore the particle size of the formed nanocomposites is changed. Moreover, much larger particle sizes were observed for the samples in which the IL was anchored on Bi and V sides simultaneously (Table S1, ESI†). The larger particle size might be related to the presence of vanadium oxide content because it increases the particle size when mixed with the Bi precursor and corroborates the higher Bi–O or V–O interaction described before

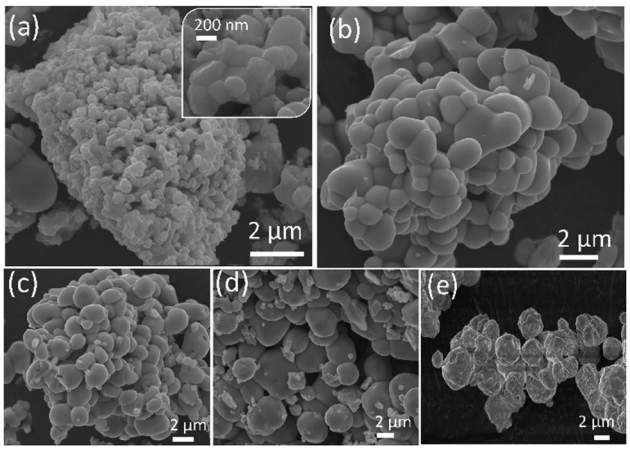

Fig. 3 SEM images of the synthesized samples with and without the ionic liquid. (a) Bi:[V–Bm], (b) Bi:[V–Me], (c) [Bi–Bm]:[V–Bm], (d) [Bi–Me]:[V–Me] and (e) pure $BiVO_4$.

(Fig. 2b).[51] For comparison, we also obtained the SEM images of HT-$BiVO_4$ and [Bi–Bm]:V in which the IL was anchored to the Bi side and NH_4VO_3 was used as the V precursor. The effect of anchoring the IL on Bi is different as a distinct morphology was obtained (Fig. S3, ESI†) when compared to Fig. 3. HT-$BiVO_4$ resulted in agglomerated microparticles with an average size of 2.3 μm.

The IL based $BiVO_4$ samples show almost the same BET specific surface area (Table S2 and Fig. S4, ESI†) which is higher compared to pure $BiVO_4$. The higher surface area may result from the increased Bi–O and V–O interactions on the surface of these materials due to the presence of ILs. These results suggest that the ILs act as templates for self-crystal organization to increase the specific surface area.

X-Ray photoelectron spectroscopy (XPS) was used to analyze the surface chemical composition and any possible BE shift related to ILs. The high resolution spectra of Bi 4f, V 2p, and O 1s are compared in Fig. 4. For pure $BiVO_4$, Bi $4f_{7/2}$ and Bi $4f_{5/2}$ corresponding to Bi^{3+} appeared at BEs of ~164.5 and ~159.2, respectively, and the peaks at ~524.4 and ~516.9 eV were assigned to V $2p_{3/2}$ and V $2p_{1/2}$, respectively, attributed to V^{5+}. These BEs correspond to the formation of $BiVO_4$.[52,53] Compared to pure $BiVO_4$, the samples prepared using the ILs presented a peak shift for Bi 4f and V 2p core levels towards higher BEs which is notably large for [Bi–Me]:[V–Me] and [Bi–Bm]:[V–Bm]. In line with the literature, the shift in the BEs indicates the oxygen vacancy generation in $BiVO_4$ due to the presence of ILs.[54] Ideally, for $BiVO_4$, the XPS peak ratio (V/Bi) is 1; however, in the literature, this has never been achieved, indicating the surface complexity of $BiVO_4$.[55,56] For the prepared samples, V/Bi relative sensitivity corrected peak area ratios are given in Table S2 (ESI†). The peak area ratios for [Bi–Me]:[V–Me] and [Bi–Bm]:[V–Bm] are increased when compared to the other samples, indicating the presence of a large amount of V species on the surface of these samples. On the other hand, for [Bi–Bm]:V, the observed peak ratio was 6.66 (Fig. S5, ESI†) which further confirms when the IL is anchored to the Bi side, a large

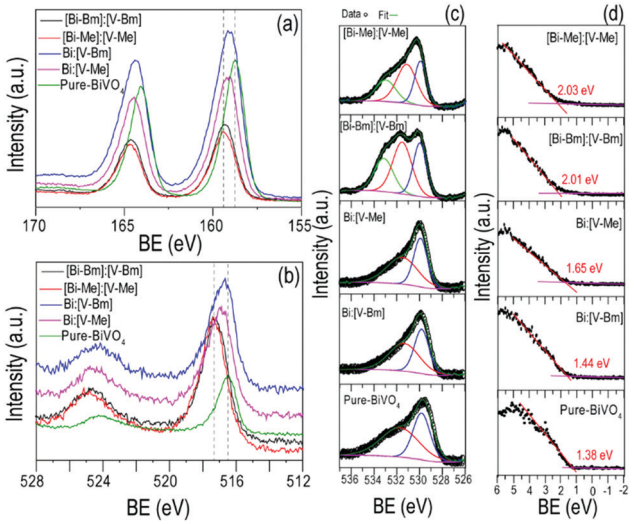

Fig. 4 XPS spectra of the (a) Bi 4f, (b) V 2p and (c) O 1s core levels of all samples and (d) their respective relative valence band positions. The dotted lines in (a) and (b) serve as a guide to the eye to observe the peak shift relative to the sample prepared without ILs.

amount of V remains on the surface. From XRD analysis (Fig. 2 and Fig. S1a, ESI†), we observed the presence of V_2O_5 and XPS analyses also show a higher content of V_2O_5 on the surface for the syntheses of samples that encompass ILs on the Bi side. In the O 1s core level (Fig. 4c), the peaks at ~529.9 and ~531.3 eV are attributed to the lattice oxygen of $BiVO_4$ and chemisorbed OH^-, respectively. These peaks were observed for all samples. The oxygen vacancies have a negligible effect on the core level O 1s BE;[57] thus, its position remains unaffected. The oxygen vacancy regions are the centers for OH species.[58] For [Bi–Me]:[V–Me] and [Bi–Bm]:[V–Bm], the peak at ~531.3 eV was also intensified. Gu *et al.* (2020) observed an increase in the amounts of superoxide radicals ($O^{2-\bullet}$) and hydroxyl radicals ($^{\bullet}OH$) for higher order oxygen vacancies in $BiVO_4$, suggesting that these samples exhibit a higher number of oxygen vacancies. An additional peak at BE ~533.2 eV was also observed for these samples (Fig. 4c). This peak may be ascribed to the physically adsorbed oxygen.[59] Fig. 4d presents the valence band (VB) XPS spectra. Interestingly, the presence of the ionic liquid has influenced the VB position. When compared to pure $BiVO_4$ and HT-$BiVO_4$, all the other samples presented an upward shift in the VB, and for [Bi–Me]:[V–Me], [Bi–Bm]:[V–Bm], and [Bi–Bm]:V (Fig. 4d and Fig. S5, ESI†), this effect was the largest. Thus, anchoring ILs on the Bi side leads to an upward shift in the VB position compared to their incorporation on the V side. The XPS results collectively show that ILs generate O vacancies; thereby, a red-shift in the bandgap (Fig. 2c) is observed due to the upward shift of the VB. Furthermore, when IL anchored Bi is mixed with the IL free V precursor or IL anchored V, the effect of generating O vacancies is profound. However, the side effect of this interaction is the low diffusibility of Bi and V, resulting in the formation of $BiVO_4$ simultaneously with V_2O_5. In addition, this results in the accumulation of oxygen species on the surface which may act as charge recombination centers for photocatalytic reactions.[59]

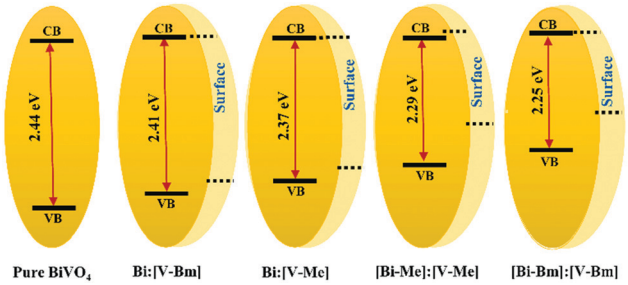

Scheme 2 The electronic structure of $BiVO_4$ prepared with different synthesis steps based on the ILs. The solid and dotted lines represent the bulk and surface CB/VB edges, respectively. The presence of ILs in the synthesis efficiently controls the electronic structure.

On the other hand, when IL anchored V is mixed with unanchored Bi (bismuth nitrate), *i.e.* the samples Bi:[V–Me] and Bi:[V–Bm], the crystal structure exhibits O vacancies but to a lower proportion when compared to [Bi–Me]:[V–Me] and [Bi–Bm]:[V–Bm]. In that case, the formation of V_2O_5 and the accumulation of surface oxygen species are also inhibited. It should also be noted that, when comparing the bandgaps (Table S2, ESI†), the highest red-shift (*ca.* 0.16 eV) was observed for [Bi–Bm]:[V–Bm] compared to pure $BiVO_4$. However, the same shift in the VB spectrum is ~0.6 eV from which we may infer that the surface exhibits a much higher number of defects than the bulk. Based on the UV-Vis and XPS results, the bulk and surface electronic structures of the samples prepared in the current work are given in Scheme 2. It can be seen that the shifts in the VB are higher compared to their bulk counterparts which are due to the produced oxygen defects through IL based synthesis.

The samples were tested for photocatalytic O_2 evolution over 3 h using radiation from a Xe lamp with a 1.5 G filter in a photolysis setup (Fig. 5). The total amounts of O_2 produced by [Bi–Bm]:V, [Bi–Me]:V, [Bi–Bm]:[V–Bm], [Bi–Me]:[V–Me] and pure $BiVO_4$ in the 3 h of reaction time are 28.6, 24.2, 16.6, 3.2 and 10.3 μmol, respectively. The sample synthesized using [BMIm] resulted in a better photocatalytic performance which can be rationalized to its higher-order crystallinity and smaller particle size. The higher the crystallinity of the samples, the greater the photocatalytic O_2 evolution which also corroborates previous

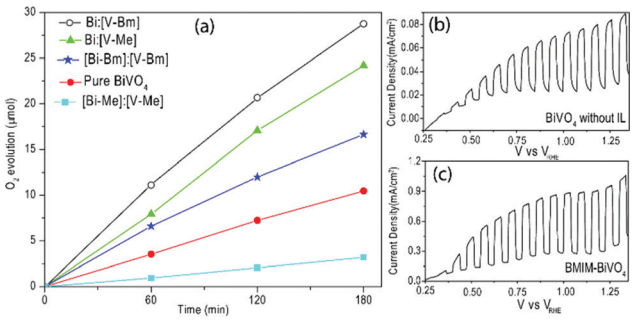

Fig. 5 (a) Oxygen evolution reaction of all samples for 3 h exposure to 300 W Xe radiation filtered with AM 1.5G. Chopped LSV curves of $BiVO_4$ synthesized (b) without and (c) with the BMIm based IL under 1 sun illumination.

reports on $BiVO_4$.[49,60] In the case of [Bi–Bm]:[V–Bm], [Bi–Me]:[V–Me] and [Bi–Bm]:V, the photoactivity was decreased, though they all presented a remarkable red-shift in the bandgap (Fig. 2c and Fig. S1b, ESI†). It is known that [M(MOE)Im] exhibits a lower microviscosity when compared to [BMIm]. In addition, the [BMIm] side chain is less polar and less flexible in contrast to [M(MOE)Im] in which the ether group oxygen acts as a hydrogen bond acceptor. Thus, the [M(MOE)Im] interaction with anions exhibits less electrostatic attraction with the cations, leading to lower structural heterogeneity.[61] Therefore, the effect of these heterogeneities of ILs results in different $BiVO_4$ structures.

It should be noted that, for these samples, the presence of V_2O_5 was observed in the XRD analyses (Fig. 2a and Fig. S1a, ESI†); in addition, chemisorbed oxygen species were also observed on their surface (Fig. 4). We may suggest that the chemisorbed oxygen species and V_2O_5 content in the oxide matrix may act as charge recombination and trapping sites for the photogenerated charge carriers. The presence of ILs helps in improving the light absorption in these syntheses *via* oxygen vacancy generation, but at the same time depending on the cationic interaction with Bi and V, the nucleation of $BiVO_4$ is also different which results in distinguished morphological, structural, and electronic properties. For comparison, we have also synthesized $BiVO_4$ based on a conventional hydrothermal process which is named HT-$BiVO_4$ (Fig. S6, ESI†). Clearly, the samples [Bi–Bm]:V and [Bi–Me]:V resulted in a better performance compared to HT-$BiVO_4$. The synthesis based on the BMIm IL resulted in enhanced oxygen evolution (Fig. 5a); therefore, we prepared $BiVO_4$ photoelectrodes using BMIm by spin coating. Fig. 5(b and c) compares the LSV curves of the prepared $BiVO_4$ with and without the IL. The PEC performance of BMIm-$BiVO_4$ is far superior to that of $BiVO_4$ prepared without the IL. It can be seen that the sample prepared with the IL presented an improved photocurrent of $\sim$1 mA cm^{-2} compared to 0.08 mA cm^{-2} of the sample prepared under the same conditions without the IL under 1 sun illumination. The MS plots (Fig. S7, ESI†) show that the flat band was not affected much due to the presence of the IL in the synthesis; however, the slopes of both plots are different, which can be attributed to different defect densities (N_D).[62,63] Based on the MS plots, the defect densities were calculated. $BiVO_4$ without the IL showed a N_D of 3.9×10^{19} cm^{-3}, whereas BMIm-$BiVO_4$ presented a N_D of 8.7×10^{20} cm^{-3}. These results show that IL based synthesis results in higher order defect generation.

The photoluminescence (PL) spectra of pure $BiVO_4$, Bi:[V–Bm] and Bi:[V–Me] excited by light of different wavelengths are shown in Fig. 6. The emission centered at $\sim$510 nm (Fig. 6a) for pure $BiVO_4$ corresponds to the electron–hole recombination.[64] At any given incident light wavelength, the fluorescence intensities for this transition were suppressed for Bi:[V–Bm] and Bi:[V–Me], indicating that IL based syntheses decrease the charge recombination compared to pure $BiVO_4$.[65] The secondary emission peaks corresponding to 380, 400 and 420 nm incident wavelengths are shown in Fig. 6d which present variations in the peak intensities. At any given incident light wavelength, the samples Bi:[V–Bm] and Bi:[V–Me] have lower intensities compared to pure $BiVO_4$ and the lowest intensity was observed for Bi:[V–Bm]. These results show that Bi:[V–Bm] exhibits improved charge transport characteristics, consequently improving the photocatalytic activity (Fig. 5) compared to all other samples.[66]

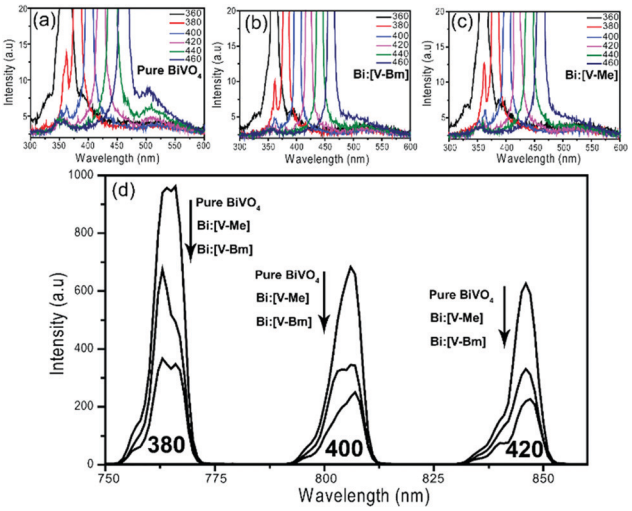

Fig. 6 PL spectra of (a) pure $BiVO_4$, (b) Bi:[V–Bm] and (c) Bi:[V–Me] excited with incident light wavelengths of 360, 380, 400, 420, 440 and 460 nm. (d) The secondary emission peaks resulting from different incident wavelengths. The incident wavelengths are given at the bottom of the peaks and arrows represent the descending order of the intensities for each sample, which is the highest for pure $BiVO_4$, followed by Bi:[V–Me] and Bi:[V–Bm].

We have conducted the stability test by illuminating Bi:[V–Bm] for 12 h continuously using AM 1.5G illumination (Fig. S9a, ESI†). The oxygen evolution was monitored by GC. The oxygen evolution rate was linear initially and decreased after 6 h. A similar behavior was observed in the literature for $BiVO_4$ in electron accepting $Fe(NO_3)_3$ (aq.) electrolyte.[67] The possible reasons for the decreasing photoactivity may be the deposition of iron species on the $BiVO_4$ surface or photodegradation of $BiVO_4$. After 12 h of irradiation, visually the sample looked darker. UV-Vis spectra were also recorded before and after the reaction (Fig. S9b, ESI†). The sample presented a decrease in the light absorption after 12 h of illumination. The bandgap energy of the sample after the test changed to 3.31 eV, which might be related to the accumulation of iron species on $BiVO_4$ or photodegradation of $BiVO_4$.[67,68] To avoid the deposition of iron species, Han *et al.* suggested adjusting the pH of the electrolyte to maintain its acidity.[67]

4. Conclusion

In summary, a new dopant-free method was developed to modify the electronic structure of $BiVO_4$. Firstly, four new Bi/V precursor ILs were prepared by modifying the anions of [BMIm][Cl] and [M(MOE)Im][Cl] namely ([BMIm][VO_3], [M(MOE)Im][VO_3], [BMIm][$BiCl_4$] and [M(MOE)Im][$BiCl_4$]). They were mixed with each other as well as with the commercially available bismuth and vanadium precursors. To obtain $BiVO_4$, these mixtures

were simply heat-treated. Choosing whether Bi or V or both sides for anchoring ILs, one can modify the morphology, crystal and electronic structures, and optical properties of $BiVO_4$. The effect of anchoring ILs to the Bi or V side resulted in modification of the electronic structure due to the upshift of the VB which induced a red-shift in the bandgap energy. Similarly, the distinct IL interaction resulted in the formation of O vacancies as observed in the XPS analyses and suppressed charge recombination as observed in the PL spectra. The effect was profound for samples in which ILs were anchored to the Bi side; however, the drawbacks of this synthesis were the formation of a higher content of V_2O_5 in the $BiVO_4$ matrix and the accumulation of chemisorbed oxygen species, which demand further research focusing on proposing additional steps to avoid these side reactions. In photolysis, improved results were obtained for samples in which ILs were anchored to the V side only, *i.e.* Bi:[V–Bm], which resulted in an almost 5-fold improvement in O_2 gas evolution compared to $BiVO_4$ prepared without ILs, which was also higher than the $BiVO_4$ prepared by the conventional hydrothermal process. Additionally, in the PEC setup improved results were also obtained from IL based synthesis compared to pure $BiVO_4$. Cationic interactions are fundamental for the modification of the electronic structure. Probably the differential lateral chain and higher order structural heterogeneity of [BMIm] compared to [M(MOE)Im] might be the reason for the better photocatalytic performance of [BMIm] based synthesis. The dopant-free approach based on ILs for modifying the electronic structure presented in this work can serve as a model for other semiconducting oxides.

Conflicts of interest

There are no conflicts to declare.

Acknowledgements

This work was conducted with the collaborative funding of Fundação de Amparo à Pesquisa do Estado do Rio Grande do Sul (FAPERGS) process no. 19/2551-0002287-5 and the São Paulo Research Foundation (FAPESP, Grant 2019/15434-2) *via* FAPERGS-FAPESP call 06/2019. The authors are also grateful to Conselho Nacional de Desenvolvimento Científico e Tecnológico (CNPq) (Process number: 306871/2021-1) and Coordenação de Aperfeiçoamento de Pessoal de Nível Superior (CAPES) (CAPES-PRINT call). The authors also acknowledge Dr Fabiano Rodembusch for conducting PL experiments.

References

1 D. G. Nocera, Solar fuels and solar chemicals industry, *Acc. Chem. Res.*, 2017, **50**, 616–619, DOI: **10.1021/ACS.ACCOUNTS.6B00615**.
2 N. S. Lewis, Developing a scalable artificial photosynthesis technology through nanomaterials by design, *Nat. Nanotechnol.*, 2016, **11**, 1010–1019, DOI: **10.1038/nnano.2016.194**.
3 N. S. Lewis, Toward Cost-Effective Solar Energy Use, *Science*, 2007, **315**, 798–801, DOI: **10.1126/science.1137014**.
4 B. A. Pinaud, J. D. Benck, L. C. Seitz, A. J. Forman, Z. Chen, T. G. Deutsch, B. D. James, K. N. Baum, G. N. Baum, S. Ardo, H. Wang, E. Miller and T. F. Jaramillo, Technical and economic feasibility of centralized facilities for solar hydrogen production via photocatalysis and photoelectrochemistry, *Energy Environ. Sci.*, 2013, **6**, 1983–2002, DOI: **10.1039/c3ee40831k**.
5 M. G. Walter, E. L. Warren, J. R. McKone, S. W. Boettcher, Q. Mi, E. A. Santori and N. S. Lewis, Solar water splitting cells, *Chem. Rev.*, 2010, **110**, 6446–6473, DOI: **10.1021/CR1002326**.
6 D. G. Nocera, The artificial leaf, *Acc. Chem. Res.*, 2012, **45**, 767–776, DOI: **10.1021/AR2003013**.
7 L. Zhang, H. Wang, Z. Chen, P. K. Wong and J. Liu, Bi2WO6 micro/nano-structures: synthesis, modifications and visible-light-driven photocatalytic applications, *Appl. Catal., B*, 2011, **106**, 1–13, DOI: **10.1016/j.apcatb.2011.05.008**.
8 M. Mao, F. Chen, C. Zheng, J. Ning, Y. Zhong and Y. Hu, Facile synthesis of porous Bi2O3-BiVO4p-n heterojunction composite microrods with highly efficient photocatalytic degradation of phenol, *J. Alloys Compd.*, 2016, **688**, 1080–1087, DOI: **10.1016/j.jallcom.2016.07.128**.
9 Y. Wang, Y. Long and D. Zhang, Novel bifunctional V_2O_5/BiVO4 nanocomposite materials with enhanced antibacterial activity, *J. Taiwan Inst. Chem. Eng.*, 2016, **68**, 387–395, DOI: **10.1016/j.jtice.2016.10.001**.
10 Z. Qiao, T. Yan, W. Li and B. Huang, In situ anion exchange synthesis of In2S3/In(OH)3 heterostructures for efficient photocatalytic degradation of MO under solar light, *New J. Chem.*, 2017, **41**, 3134–3142, DOI: **10.1039/c6nj04119a**.
11 A. Malathi, V. Vasanthakumar, P. Arunachalam, J. Madhavan and M. A. Ghanem, A low cost additive-free facile synthesis of BiFeWO6/BiVO4 nanocomposite with enhanced visible-light induced photocatalytic activity, *J. Colloid Interface Sci.*, 2017, **506**, 553–563, DOI: **10.1016/j.jcis.2017.07.079**.
12 S. Khan, T. Lemes Ruwer, N. Khan, A. Köche, R. W. Lodge, H. Coelho-Júnior, R. L. Sommer, M. J. Leite Santos, C. F. Malfatti, C. P. Bergmann and J. A. Fernandes, Revealing the true impact of interstitial and substitutional nitrogen doping in TiO_2 on photoelectrochemical applications, *J. Mater. Chem. A*, 2021, **9**, 12214–12224, DOI: **10.1039/d0ta11494d**.
13 H. Ullah, A. Ur Rahman, E. Leonetti Aragão, F. Fróis Alves Barbosa, K. Gabriel Ramisch Pergher, R. Giulian, H. Coelho Júnior, R. Luis Sommer and S. Khan, Homogeneous V incorporation via single-step anodization: structural doping or heterostructure formation?, *Appl. Surf. Sci.*, 2021, **556**, 149694, DOI: **10.1016/j.apsusc.2021.149694**.
14 S. Khan, M. J. M. Zapata, D. L. Baptista, R. V. Gonçalves, J. A. Fernandes, J. Dupont, M. J. L. Santos and S. R. Teixeira, Effect of Oxygen Content on the Photoelectrochemical Activity of Crystallographically Preferred Oriented Porous Ta_3N_5 Nanotubes, *J. Phys. Chem. C*, 2015, **119**, 19906–19914, DOI: **10.1021/ACS.JPCC.5B05475**.
15 Y. Hu, J. Fan, C. Pu, H. Li, E. Liu and X. Hu, Facile synthesis of double cone-shaped $Ag_4V_2O_7$/$BiVO_4$ nanocomposites

with enhanced visible light photocatalytic activity for environmental purification, *J. Photochem. Photobiol., A*, 2017, **337**, 172–183, DOI: 10.1016/j.jphotochem.2016.12.035.

16 D. Lv, D. Zhang, X. Pu, D. Kong, Z. Lu, X. Shao, H. Ma and J. Dou, One-pot combustion synthesis of $BiVO_4$/BiOCl composites with enhanced visible-light photocatalytic properties, *Sep. Purif. Technol.*, 2017, **174**, 97–103, DOI: 10.1016/j.seppur.2016.10.010.

17 M. Guo, Y. Wang, Q. He, W. Wang, W. Wang, Z. Fu and H. Wang, Enhanced photocatalytic activity of S-doped $BiVO_4$ photocatalysts, *RSC Adv.*, 2015, **5**, 58633–58639, DOI: 10.1039/c5ra07603j.

18 L. Zhou, W. Wang, S. Liu, L. Zhang, H. Xu and W. Zhu, A sonochemical route to visible-light-driven high-activity $BiVO_4$ photocatalyst, *J. Mol. Catal. A: Chem.*, 2006, **252**, 120–124, DOI: 10.1016/j.molcata.2006.01.052.

19 F. F. Abdi and R. Van De Krol, Nature and light dependence of bulk recombination in Co–Pi-catalyzed $BiVO_4$ photoanodes, *J. Phys. Chem. C*, 2012, **116**, 9398–9404, DOI: 10.1021/JP3007552.

20 H. L. Tan, R. Amal and Y. H. Ng, Alternative strategies in improving the photocatalytic and photoelectrochemical activities of visible light-driven $BiVO_4$: a review, *J. Mater. Chem. A*, 2017, **5**, 16498–16521, DOI: 10.1039/c7ta04441k.

21 Y. Ma, S. R. Pendlebury, A. Reynal, F. Le Formal and J. R. Durrant, Dynamics of photogenerated holes in undoped $BiVO_4$ photoanodes for solar water oxidation, *Chem. Sci.*, 2014, **5**, 2964–2973, DOI: 10.1039/c4sc00469h.

22 T. S. Sinclair, B. M. Hunter, J. R. Winkler, H. B. Gray and A. M. Müller, Factors affecting bismuth vanadate photoelectrochemical performance, *Mater. Horizons.*, 2015, **2**, 330–337, DOI: 10.1039/c4mh00156g.

23 E. A. Mohamed, Z. N. Zahran and Y. Naruta, Simple preparation of highly active water splitting FTO/$BiVO_4$ photoanode modified with tri-layer water oxidation catalysts, *J. Mater. Chem. A*, 2017, **5**, 6825–6831, DOI: 10.1039/c7ta00156h.

24 D. K. Zhong, S. Choi and D. R. Gamelin, Near-complete suppression of surface recombination in solar photoelectrolysis by "co-Pi" catalyst-modified W:$BiVO_4$, *J. Am. Chem. Soc.*, 2011, **133**, 18370–18377, DOI: 10.1021/JA207348X.

25 S. Wang, T. He, J. H. Yun, Y. Hu, M. Xiao, A. Du and L. Wang, New Iron-Cobalt Oxide Catalysts Promoting $BiVO_4$ Films for Photoelectrochemical Water Splitting, *Adv. Funct. Mater.*, 2018, **28**(34), 1802685, DOI: 10.1002/ADFM.201802685.

26 B. Zhou, X. Zhao, H. Liu, J. Qu and C. P. Huang, Synthesis of visible-light sensitive M-$BiVO_4$ (M = Ag, Co, and Ni) for the photocatalytic degradation of organic pollutants, *Sep. Purif. Technol.*, 2011, **77**, 275–282, DOI: 10.1016/j.seppur.2010.12.017.

27 M. Zhou, J. Bao, Y. Xu, J. Zhang, J. Xie, M. Guan, C. Wang, L. Wen, Y. Lei and Y. Xie, Photoelectrodes based upon Mo:$BiVO_4$ inverse opals for photoelectrochemical water splitting, *ACS Nano*, 2014, **8**, 7088–7098, DOI: 10.1021/NN501996A.

28 F. F. Abdi, L. Han, A. H. M. Smets, M. Zeman, B. Dam and R. Van De Krol, Efficient solar water splitting by enhanced charge separation in a bismuth vanadate-silicon tandem photoelectrode, *Nat. Commun.*, 2013, **4**, 2195, DOI: 10.1038/ncomms3195.

29 X. Shi, I. Y. Choi, K. Zhang, J. Kwon, D. Y. Kim, J. K. Lee, S. H. Oh, J. K. Kim and J. H. Park, Efficient photoelectrochemical hydrogen production from bismuth vanadate-decorated tungsten trioxide helix nanostructures, *Nat. Commun.*, 2014, **5**, 4775, DOI: 10.1038/ncomms5775.

30 M. Antonietti, D. Kuang, B. Smarsly and Y. Zhou, Ionic liquids for the convenient synthesis of functional nanoparticles and other inorganic nanostructures, *Angew. Chem., Int. Ed.*, 2004, **43**, 4988–4992, DOI: 10.1002/anie.200460091.

31 J. A. Dahl, B. L. S. Maddux and J. E. Hutchison, Toward greener nanosynthesis, *Chem. Rev.*, 2007, **107**, 2228–2269, DOI: 10.1021/CR050943K.

32 M. Zhen, J. Yu and S. Dai, Preparation of inorganic materials using ionic liquids, *Adv. Mater.*, 2010, **22**, 261–285, DOI: 10.1002/ADMA.200900603.

33 J. Dupont, C. S. Consorti, P. A. Z. Suarez and R. F. de Souza, Preparation of 1-Butyl-3-Methyl Imidazolium-Based Room Temperature Ionic Liquids, *Org. Synth.*, 2003, 236, DOI: 10.1002/0471264180.OS079.28.

34 G. Chacón and J. Dupont, Arene Hydrogenation by Metal Nanoparticles in Ionic Liquids, *ChemCatChem*, 2019, **11**, 333–341, DOI: 10.1002/CCTC.201801363.

35 A. G. Wallace and M. D. Symes, Water-Splitting Electrocatalysts Synthesized Using Ionic Liquids, *Trends Chem.*, 2019, **1**, 247–258, DOI: 10.1016/j.trechm.2019.03.003.

36 H. Weber and B. Kirchner, Ionic Liquid Induced Band Shift of Titanium Dioxide, *ChemSusChem*, 2016, **9**, 2505–2514, DOI: 10.1002/CSSC.201600844.

37 M. I. Qadir, M. Zanatta, J. Pinto, I. Vicente, A. Gual, E. F. Smith, B. A. D. Neto, P. E. N. de Souza, S. Khan, J. Dupont and J. Alves Fernandes, Reverse Semi-Combustion Driven by Titanium Dioxide-Ionic Liquid Hybrid Photocatalyst, *ChemSusChem*, 2020, **13**, 5580–5585, DOI: 10.1002/cssc.202001717.

38 Q. Zhang, M. Liu, W. Zhou, Y. Zhang, W. Hao, Y. Kuang, H. Liu, D. Wang, L. Liu and J. Ye, A novel Cl- modification approach to develop highly efficient photocatalytic oxygen evolution over $BiVO_4$ with AQE of 34.6%, *Nano Energy*, 2021, **81**, 105651, DOI: 10.1016/j.nanoen.2020.105651.

39 (*a*) W. Han, H. Lin, F. Fang, Y. Zhang, K. Zhang, X. Yu and K. Chang, The effect of Fe(III) ions on oxygen-vacancy-rich $BiVO_4$ on the photocatalytic oxygen evolution reaction, *Catal. Sci. Technol.*, 2021, **11**, 7598–7607, DOI: 10.1039/D1CY01559A; (*b*) Z. Qiang, J. Huang, C. Yang, F. Li, T. Li, M. Huttula, Z. Huang and W. Cao, A Facile Synthesis of Heterojunctional $BiVO_4$/Bi5O7I with Enhanced Photocatalytic Activity for Organic Dyes Degradation, *J. Inorg. Organomet. Polym.*, 2020, **30**, 1829–1838, DOI: 10.1007/S10904-019-01348-0; (*c*) C. Yang, F. Li and T. Li, A one-step ionic liquid-assisted ultrasonic method for the preparation of BiOCl/m-$BiVO_4$ heterojunctions with enhanced visible light photocatalytic activity, *CrystEngComm*, 2015, **17**, 7676–7683, DOI: 10.1039/C5CE01312G.

40 S. Hameury, P. De Frémont, P. A. R. Breuil, H. Olivier-Bourbigou and P. Braunstein, Bis(ether-functionalized NHC) Nickel(II) Complexes, Trans to Cis Isomerization Triggered by Water Coordination, and Catalytic Ethylene Oligomerization, *Organometallics*, 2015, **34**, 2183–2201, DOI: 10.1021/OM5008506.

41 M. A. Melo, H. A. Centurion, T. T. A. Lucas, D. N. F. Muche, F. L. Souza and R. V. Gonçalves, Pseudobrookite Fe2TiO5-Nanoparticles Loaded with Earth-Abundant Nanosized NiO and Co3O4Cocatalysts for Photocatalytic O2Evolution via Solar Water Splitting, *ACS Appl. Nano Mater.*, 2020, **3**, 9303–9317, DOI: 10.1021/ACSANM.0C01957.

42 P. Pookmanee, S. Kojinok and S. Phanichphant, Bismuth vanadate ($BiVO_4$) powder prepared by the sol-gel method, *J. Met., Mater. Miner.*, 2012, **22**, 49–53, http://www.jmmm.material.chula.ac.th/index.php/jmmm/article/view/49, accessed December 23, 2021.

43 S. M. Thalluri, C. Martinez Suarez, S. Hernández, S. Bensaid, G. Saracco and N. Russo, Elucidation of important parameters of $BiVO_4$ responsible for photo-catalytic O2 evolution and insights about the rate of the catalytic process, *Chem. Eng. J.*, 2014, **245**, 124–132, DOI: 10.1016/j.cej.2014.02.017.

44 R. Rowe, K. R. J. Lovelock and P. A. Hunt, Bi(III) halometallate ionic liquids: Interactions and speciation, *J. Chem. Phys.*, 2021, **155**, 014501, DOI: 10.1063/5.0052297.

45 D. S. Su and R. Schlögl, Thermal decomposition of divanadium pentoxide V_2O_5: towards a nanocrystalline V_2O_3 phase, *Catal. Lett.*, 2002, **83**, 115–119, DOI: 10.1023/A:1021042232178.

46 A. Galembeck and O. L. Alves, Bismuth vanadate synthesis by metallo-organic decomposition: Thermal decomposition study and particle size control, *J. Mater. Sci.*, 2002, **37**, 1923–1927, DOI: 10.1023/A:1015206426473.

47 J. I. Langford and A. J. C. Wilson, Scherrer after sixty years: A survey and some new results in the determination of crystallite size, *J. Appl. Crystallogr.*, 1978, **11**, 102–113, DOI: 10.1107/S0021889878012844.

48 Y. K. Kho, W. Y. Teoh, A. Iwase, L. Mädler, A. Kudo and R. Amal, Flame preparation of visible-light-responsive BiVO 4 oxygen evolution photocatalysts with subsequent activation via aqueous route, *ACS Appl. Mater. Interfaces*, 2011, **3**, 1997–2004, DOI: 10.1021/AM200247Y.

49 S. M. Thalluri, C. Martinez Suarez, M. Hussain, S. Hernandez, A. Virga, G. Saracco and N. Russo, Evaluation of the Parameters Affecting the Visible-Light-Induced Photocatalytic Activity of Monoclinic $BiVO_4$ for Water Oxidation, *Ind. Eng. Chem. Res.*, 2013, **52**, 17414–17418, DOI: 10.1021/ie402930x.

50 (*a*) M. Wang, Y. Che, C. Niu, M. Dang and D. Dong, Effective visible light-active boron and europium co-doped $BiVO_4$ synthesized by sol-gel method for photodegradion of methyl orange, *J. Hazard. Mater.*, 2013, **262**, 447–455, DOI: 10.1016/j.jhazmat.2013.08.063; (*b*) K. Biswas, Use of ionic liquids in the synthesis of nanocrystals and nanorods of semiconducting metal chalcogenides, *Chem. – Eur. J.*, 2007, **13**, 6123–6129, DOI: 10.1002/chem.200601733; (*c*) H. L. Tan, R. Amal and Y. H. Ng, Exploring the Different Roles of Particle Size in Photoelectrochemical and Photocatalytic Water Oxidation on $BiVO_4$, *ACS Appl. Mater. Interfaces*, 2016, **8**, 28607–28614, DOI: 10.1021/ACSAMI.6B09076.

51 A. Iwase, H. Kato and A. Kudo, A Simple Preparation Method of Visible-Light-Driven $BiVO_4$ Photocatalysts From Oxide Starting Materials (Bi2O3 and V_2O_5) and Their Photocatalytic Activities, *J. Sol. Energy Eng.*, 2010, **132**, 0211061–0211065, DOI: 10.1115/1.4001172.

52 J. Su, X. X. Zou, G. D. Li, X. Wei, C. Yan, Y. N. Wang, J. Zhao, L. J. Zhou and J. S. Chen, Macroporous V_2O_5–$BiVO_4$ composites: Effect of heterojunction on the behavior of photogenerated charges, *J. Phys. Chem. C*, 2011, **115**, 8064–8071, DOI: 10.1021/JP200274K.

53 A. P. Singh, N. Kodan, A. Dey, S. Krishnamurthy and B. R. Mehta, Improvement in the structural, optical, electronic and photoelectrochemical properties of hydrogen treated bismuth vanadate thin films, *Int. J. Hydrogen Energy*, 2015, **40**, 4311–4319, DOI: 10.1016/j.ijhydene.2015.01.085.

54 D. P. Jaihindh, B. Thirumalraj, S.-M. Chen, P. Balasubramanian and Y.-P. Fu, Facile synthesis of hierarchically nanostructured bismuth vanadate: an efficient photocatalyst for degradation and detection of hexavalent chromium, *J. Hazard. Mater.*, 2019, **367**, 647–657, DOI: 10.1016/j.jhazmat.2019.01.017.

55 V. Nair, C. L. Perkins, Q. Lin and M. Law, Textured nanoporous Mo:$BiVO_4$ photoanodes with high charge transport and charge transfer quantum efficiencies for oxygen evolution, *Energy Environ. Sci.*, 2016, **9**, 1412–1429, DOI: 10.1039/C6EE00129G.

56 J. Liu, K. Tajima, I. Abdellaoui, M. M. Islam, S. Ikeda and T. Sakurai, Effect of Radio-Frequency Power on the Composition of $BiVO_4$ Thin-Film Photoanodes Sputtered from a Single Target, *Energies*, 2021, **14**, 2122, DOI: 10.3390/en14082122.

57 A. Posada-Borbón, N. Bosio and H. Grönbeck, On the signatures of oxygen vacancies in O1s core level shifts, *Surf. Sci.*, 2021, **705**, 121761, DOI: 10.1016/j.susc.2020.121761.

58 G. Rahman, A. Akhtar, N. A. Khan, S. Y. Chae, A. U. H. A. Shah and O. Joo, Direct growth of duel-faceted $BiVO_4$ microcrystals on FTO-coated glass for photoelectrochemical water oxidation, *Optik*, 2020, **224**, 165516, DOI: 10.1016/j.ijleo.2020.165516.

59 D. P. Jaihindh, B. Thirumalraj, S.-M. Chen, P. Balasubramanian and Y.-P. Fu, Facile synthesis of hierarchically nanostructured bismuth vanadate: an efficient photocatalyst for degradation and detection of hexavalent chromium, *J. Hazard. Mater.*, 2019, **367**, 647–657, DOI: 10.1016/j.jhazmat.2019.01.017.

60 L. Qi, J. Yu and M. Jaroniec, Enhanced and suppressed effects of ionic liquid on the photocatalytic activity of TiO_2, *Adsorption*, 2013, **19**, 557–561, DOI: 10.1007/s10450-013-9478-7.

61 B.-X. Li, Q.-J. Guo and A.-D. Xia, Spectroscopic Study of the Structural Heterogeneity and Microviscosity of [bmim][PF6]

and [moemim][PF6] Ionic Liquids, *Acta Phys.–Chim. Sin.*, 2015, **31**, 1452–1460, DOI: **10.3866/PKU.WHXB201506101**.

62 S. Khan, S. R. Teixeira and M. J. L. Santos, Controlled thermal nitridation resulting in improved structural and photoelectrochemical properties from Ta_3N_5 nanotubular photoanodes, *RSC Adv.*, 2015, **5**, 103284–103291, DOI: **10.1039/C5RA17227F**.

63 S. Khan, M. J. L. Santos, C. F. Malfatti, J. Dupont and S. R. Teixeira, Pristine Ta3N5Nanotubes: Trap-Driven High External Biasing Perspective in Semiconductor/Electrolyte Interfaces, *Chem. – Eur. J.*, 2016, **22**, 18501–18511, DOI: **10.1002/chem.201603246**.

64 Y. Wang, W. Wang, H. Mao, Y. Lu, J. Lu, J. Huang, Z. Ye and B. Lu, Electrostatic Self-Assembly of $BiVO_4$–Reduced Graphene Oxide Nanocomposites for Highly Efficient Visible Light Photocatalytic Activities, *ACS Appl. Mater. Interfaces*, 2014, **6**, 12698–12706, DOI: **10.1021/am502700p**.

65 V. Rathi, A. Panneerselvam and R. Sathiyapriya, A novel hydrothermal induced $BiVO_4$/g-C3N4 heterojunctions visible-light photocatalyst for effective elimination of aqueous organic pollutants, *Vacuum*, 2020, **180**, 109458, DOI: **10.1016/j.vacuum.2020.109458**.

66 A. R. Nanakkal and L. K. Alexander, Graphene/$BiVO_4$/TiO2 nanocomposite: tuning band gap energies for superior photocatalytic activity under visible light, *J. Mater. Sci.*, 2017, **52**, 7997–8006, DOI: **10.1007/S10853-017-1002-0**.

67 W. Han, H. Lin, F. Fang, Y. Zhang, K. Zhang, X. Yu and K. Chang, The effect of Fe(iii) ions on oxygen-vacancy-rich $BiVO_4$on the photocatalytic oxygen evolution reaction, *Catal. Sci. Technol.*, 2021, **11**, 7598–7607, DOI: **10.1039/D1CY01559A**.

68 J. H. Kim, *et al.*, Palladium oxide as a novel oxygen evolution catalyst on $BiVO_4$ photoanode for photoelectrochemical water splitting, *J. Catal.*, 2014, **317**, 126–134, DOI: **10.1016/j.jcat.2014.06.015**.

†Electronic supporting information

Dopant-free band edge shift in $BiVO_4$ particles for enhanced oxygen evolution under simulated sunlight

Niqab Khan,*[a] Rogério Nunes Wolff,[a] Hameed Ullah,[a] Gustavo J. Chacón,[b] Washington Santa Rosa,[c] Jairton Dupont,[b] Renato Vitalino Gonçalves,[c] Sherdil Khan,*[a]

[a] Laboratory of Nanomaterials for Renewable Energy and Artificial Photosynthesis (NanoREAP), Programa de Pós-Graduação em Física (PPGFis), Federal University of Rio Grande do Sul (UFRGS), Campus do Vale, Agronomia, Porto Alegre-RS, Brazil.

[b] Laboratory of Molecular Catalysis (LAMOCA), Programa de Pós-Graduação em Química (PPQ), Federal University of Rio Grande do Sul (UFRGS), Campus do Vale, Agronomia, Porto Alegre-RS, Brazil.

[c] Laboratory of Artificial Photosynthesis (LAPA), Institute of Physics of São Carlos, University of São Paulo (USP), São Paulo, Brazil.

* sherdil.khan@ufrgs.br

Table S1. Crystalline (based on XRD analyses) and morphological (based on SEM images) properties of synthesized $BiVO_4$ through [BMIm] and [M(MOE)Im] based ionic liquids.

Sample	Crystallite size (nm)	Crystallinity (100%)	Particle size (nm)
Pure $BiVO_4$	11	54	2725±86
Bi:[V-Bm]	18	86	221±30
Bi:[V-Me]	18	76	980±62
[Bi-Bm]:[V-Bm]	19	*	1733±72
[Bi-Me]:[V-Me]	19	*	3236±47

**Additional peaks of V_2O_5 were observed which affect the crystallinity (%) calculations; therefore, their crystallinity was not calculated.*

Table S2. Raman shift and (V-O) bond length (Figure S4), surface area (Figure S4), bandgap (Figure 2c), V/B ratio (Figure 4) and oxygen evolution (Figure 5) of synthesized $BiVO_4$ with different ionic liquids

Entry	Sample	Raman shift (cm^{-1})	V-O length (Å)	S_{BET} (m^2/g)	Bandgap (eV)	V/B ratio	O_2 Evolution (µmol)
1	Bi:[V-Bm]	826.67	1.6961	11.43	2.41	0.51	28.6
2	[Bi-Bm]:[V-Bm]	828.24	1.6950	11.66	2.25	1.56	16.6
3	Bi:[V-Me]	824.90	1.6971	11.79	2.37	0.69	24.2
4	[Bi-Me]:[V-Me]	827.63	1.6955	11.10	2.29	1.72	3.2
5	Pure $BiVO_4$	828.91	1.6947	*	2.44	0.64	10.3

*Less than the instrument limit.

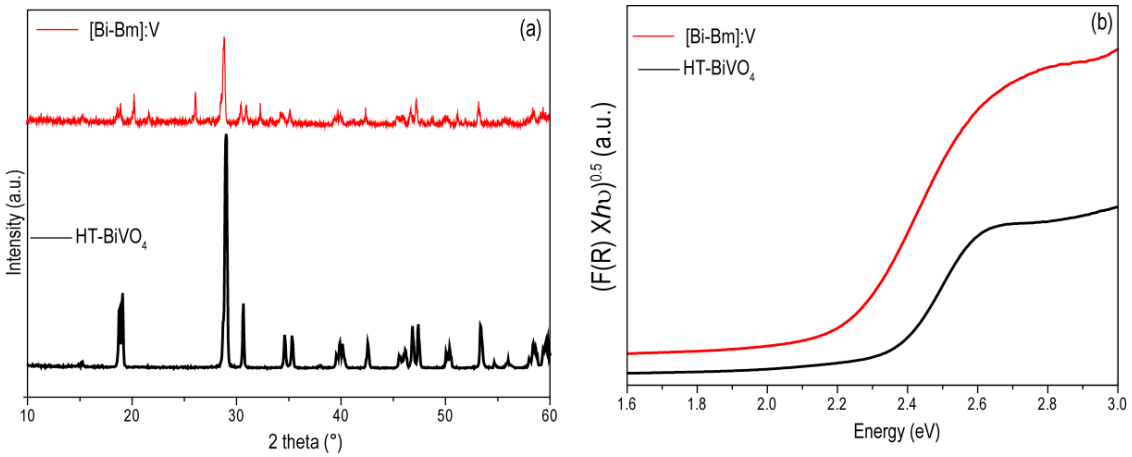

Figure S1. (a) XRD patterns and (b) UV –Vis diffused reflectance of [Bi-Bm]:V in which [BMIm] based IL anchored Bi was mixed with NH_4VO_3 to form $BiVO_4$ and HT-$BiVO_4$ prepared by conventional hydrothermal process.

Figure S1 displays the XRD patterns of [Bi-Bm]:V and HT-$BiVO_4$. For [Bi-Bm]:V in addition to $BiVO_4$ ((JCPDS) Card No. 14-0688), peaks at 2θ ~ 20°, 26° and 31° were also observed which correspond to V_2O_5. Furthermore, as compared to [Bi-Bm]:[V-Bm], and [Bi-Me]:[V-Me] (Figure 2), the relative peaks intensities of V_2O_5 was higher for [Bi-Bm]:V, indicating the formation of larger content of V_2O_5. Thus, anchoring IL with Bi side for the formation of $BiVO_4$ strongly decreases the diffusibility of Bi with V for the complete formation of $BiVO_4$. However, this synthesis results in large O defects,

thereby a notable red-shift in the bandgap was clearly observed as compared to HT-$BiVO_4$ (Figure S1b) and pure $BiVO_4$ (Figure 5).

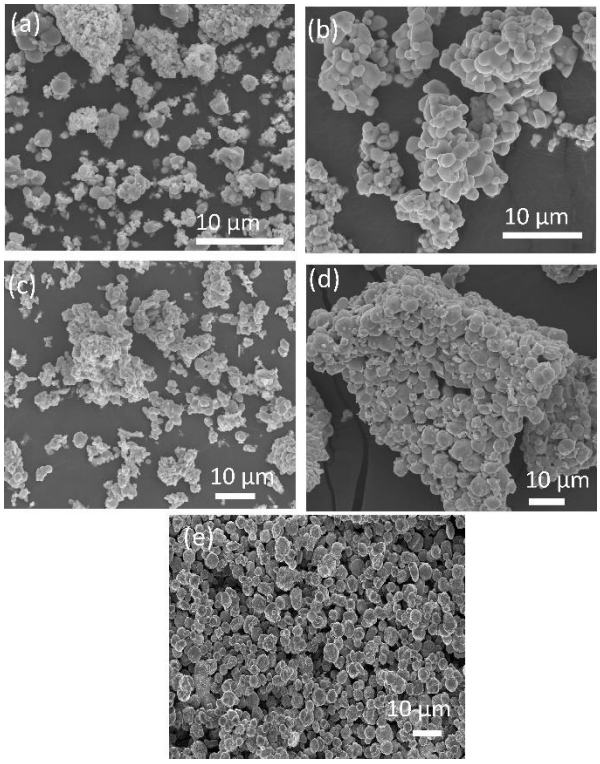

Figure S2. SEM images of the synthesized samples with and without ionic liquid. (a) Bi:[V-Bm], (b) Bi:[V-Me], (c) [Bi-Bm]:[V-Bm], (d) [Bi-Me]:[V-Me] and (e) Pure $BiVO_4$.

Figure S2 compares the low magnification images of the prepared samples, the higher magnification SEM are presented in Figure 3. As compared to pure $BiVO_4$, the samples prepared by IL presents smooth particles.

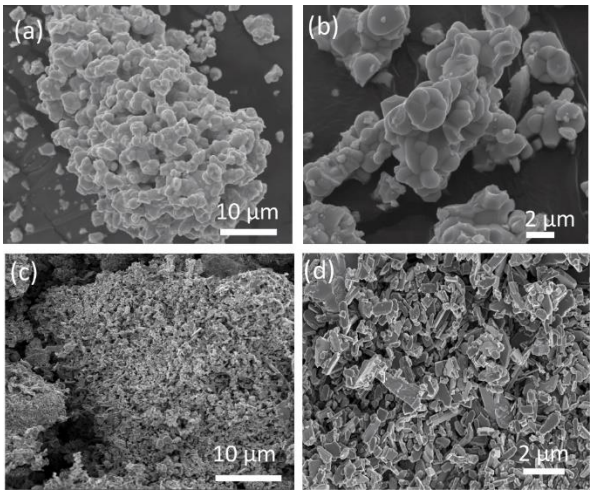

Figure S3, SEM images of (a-b) [Bi-Bm]:V in which [BMIm] based IL anchored Bi was mixed with NH_4VO_3 to form $BiVO_4$ and (c-d) HT-$BiVO_4$ prepared by conventional hydrothermal process.

Figure S3 (a-b) displays the SEM images of HT-$BiVO_4$; showing the obtained morphology is agglomerated microparticles. IL based synthesized [Bi-Bm]:V resulted into a totally different morphology (Figure S2 (c,d)) than HT-$BiVO_4$ and also as compared to all other samples (Figure 3).

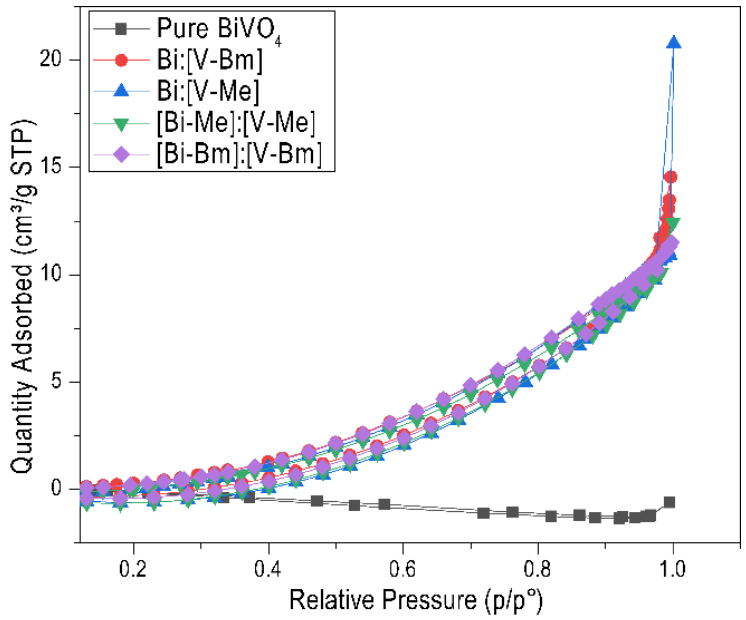

Figure S4. BET adsorption-desorption isotherms of the samples prepared with and without IL.

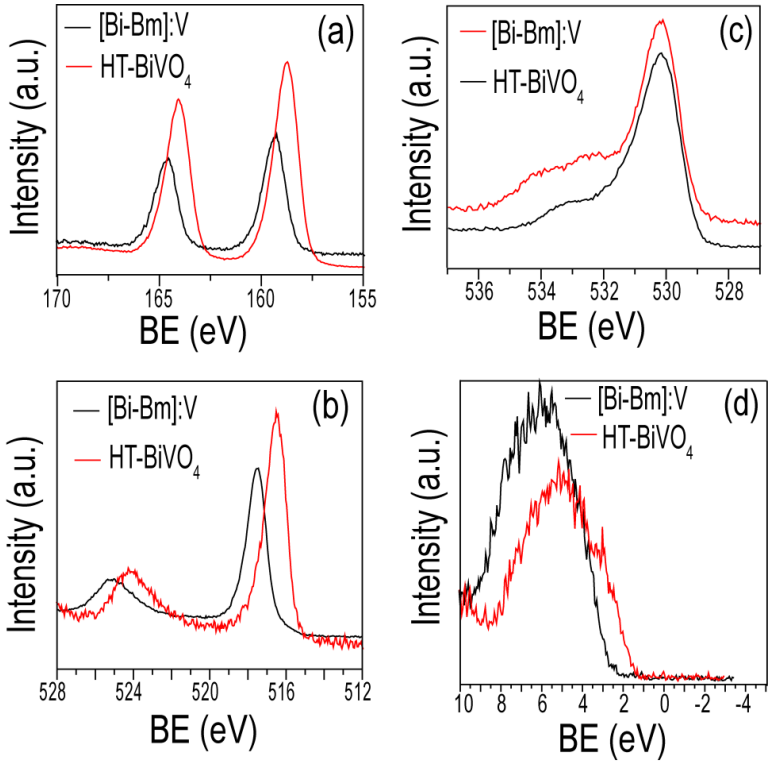

Figure S5. XPS spectra of the (a) Bi 4f, (b) V 2p and (c) O 1s core levels of [Bi-Bm]:V and HT-$BiVO_4$ and (d) their respective VB spectra. A clear peak shift in Bi df, V2p and VB can be observed for [Bi-Bm]:V as compared to HT-$BiVO_4$.

Figure S5 displays XPS spectra of [Bi-Bm]:V and HT-$BiVO_4$. The peaks positions of HT-$BiVO_4$ does not differ from pure $BiVO_4$ (Figure 4). A clear blue-shift is observed for [Bi-Bm]:V as compared to HT-$BiVO_4$ for Bi 4f, V2p and VB spectra. These results also agree with Figure 5 where blue-shift was clearly observed for IL based syntheses as compared to pure $BiVO_4$. In addition, the O1s spectra of [Bi-Bm]:V (Figure S1c) is also similar to [Bi-Bm]:[V-Bm] and [Bi-Me]:[V-Me] which present an additional peak at BE~533.2 eV corresponding to chemisorbed oxygen species. Hence anchoring IL to Bi side improves the light abosrbption by upshifting the VB but with a drawback of low reactivity of Bi with V and accumulation of O species on $BiVO_4$ surface.

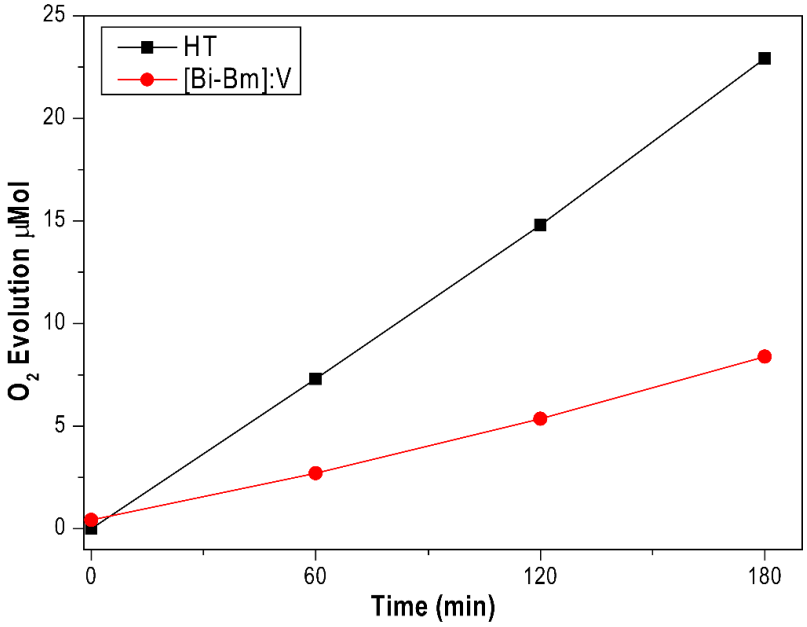

Figure S6. Oxygen evolution of [Bi-Bm]:V and HT-$BiVO_4$ for 3h exposure to 300 W Xe radiations filtered with AM 1.5G.

Figure S4 displays oxygen evolution of [Bi-Bm]:V and HT-$BiVO_4$ under simulated sunlight. Though [Bi-Bm]:V presented large absorption in the visible light, however due to accumulation of O species and presence of V_2O_5 could not perform better as compared to HT-$BiVO_4$ and pure $BiVO_4$ (Figure 5a).

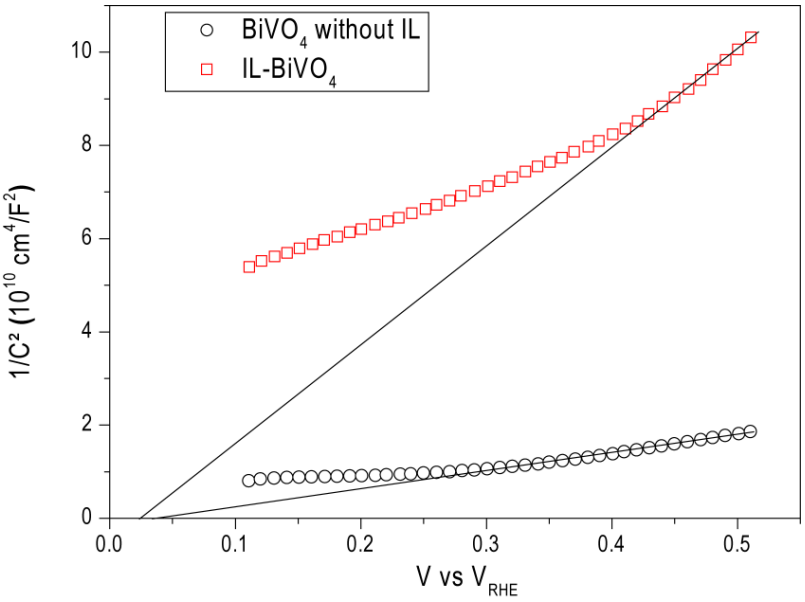

Figure S7. Mott-Schottky plots of $BiVO_4$ (prepared without IL) and BMIm-$BiVO_4$ prepared by BMIm based IL.

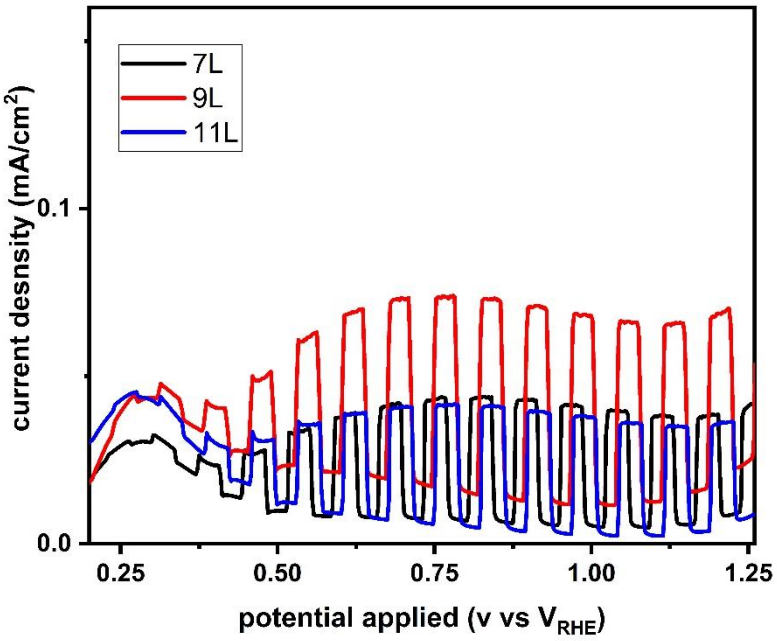

Figure S8. Chopped LSV curves of Bi:[V-Bm] with different layers i.e. 7L, 9L and 11L under 1 Sun illumination.

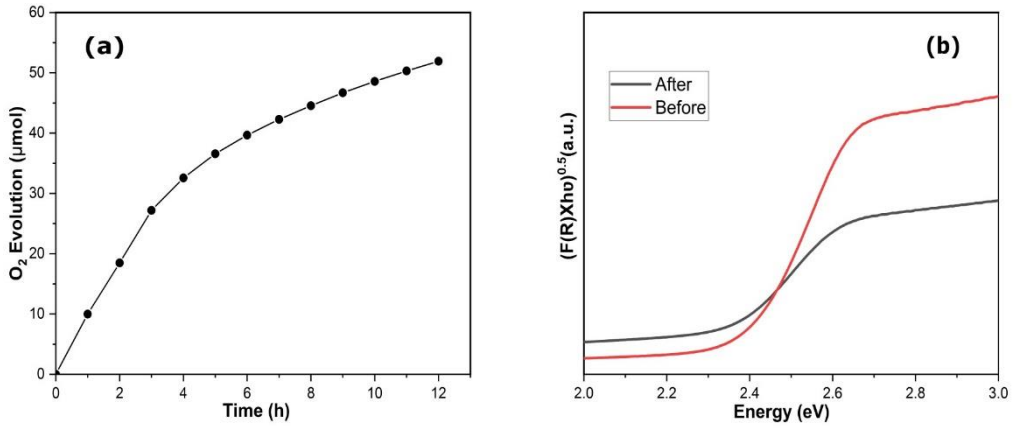

Figure S9: (a) Long time photochemical water oxidation activity of Bi:[V-Bm] at AM 1.5 illumination in 0.05 M of $Fe(NO_3)_3.9H_2O$. (b) UV –Vis diffused reflectance of Bi:[V-Bm] before and after 12h photocatalytic oxygen evolution test.